Indian Journal of Chemistry
Vol. 61, December 2022, pp. 1278- 1287
DOI: 10.56042/ijc.v61i12.69443

Synthesis, experimental and theoretical characterization with inhibitor activity for 1,2,4-traizaol derivatives

Rebaz A Omer [a,*], Pelin Koparir[b] & Metin Koparir[c]

[a]Department of Chemistry, Faculty of Science & Health, Koya University, Koya KOY45, Kurdistan Region – F.R. Iraq

[b]Forensic Medicine Institute, Department of Chemistry, Firat University, 23169, Elazig, Turkey

[c]Firat University, Faculty of Science, Department of Chemistry, 23169, Elazig, Turkey

* E-mail: rebaz.anwar@koyauniversity.org

Received 30 June 2021; accepted (revised) 18 November 2022

This study aims to synthesize and identify both theoretically and experimentally 4-phenyl-5-(thiophene-2-yl)-4H-1,2,4-triazole-3-thiol and 4-ethyl-5-(thiophene-2-yl)-4H-1,2,4-triazole-3-thiol compounds. Experimentally, FT-IR and NMR techniques have been used to characterize the synthesized compounds. The density functional theory with the basis set of cc-pVDZ have been utilized for measuring the molecular geometry, vibrational frequencies, and gauge including atomic orbital (GIAO) ^{1}H and ^{13}C NMR chemical shifts of the title compound in the ground state. The results have shown that the optimized geometry replicate the theoretical vibrations and the calculated chemical shift in line with the experimental values are in good harmony. B3LYP/cc-pVDZ was applied to the aforementioned compound to find different parameters such as the energy of the highest occupied and lower unoccupied molecular orbital (E_{HOMO} and E_{LUMO}), moreover, the bandgap energy (ΔE) and the dipole moment (μ) are calculated for the corrosion efficacy of organic compounds whose molecular geometry and electronic properties have been previously studied. Properties such as hardness (η), softness (σ), electronegativity (χ) values are computed using the respective measurements to investigate the inhibitor activity of the compound. The fraction of transferred electrons (ΔN) is also calculated, which determined the interaction between the iron surface and the organic compounds. Corrosion inhibitor behavior can therefore be predicted without an experimental study. The findings of the calculations show good relation between organic-based corrosion inhibitors and quantum chemical parameters process.

Keywords: Synthesis, Density function theory, 4-phenyl-5-(thiophene-2-yl)-4H-1,2,4-triazole-3-thiol, 4-ethyl-5-(thiophene-2-yl)-4H-1,2,4-triazole-3-thiol, Corrosion Inhibitory Activity, Electronic Properties

In recent years, research into heterocyclic molecules containing five 1,2,4 triazole rings has been increasingly developed. For the first time, in 1864, Hugo Schiff synthesized Schiff bases[1]. Schiff base occurs in the first step, where the intermediate carbonyl amine is formed from the condensation of the carbonyl group with the primary amine. In the second step, the Schiff base is formed at the end of the dehydration of the carbonyl amine intermediate compound[2]. Schiff bases are used in many scientific areas, including human and industrial fields[3-7]. Schiff bases have important inhibitor productivities at different concentrations[8-11]. Besides, the double and triple bonds, which are adsorbed on organic molecules containing phosphorus, sulfur, oxygen, and nitrogen as hetero-atoms, are effective as corrosion inhibitors[12-17]. The base molecules have an imine group that is absorbable on the surface[18, 19]. The inhibitory molecules, steric factor, aromatization and electron densities of the donor site, functional group, and also the polarization of the collective, can be used to determine the adsorption capacity of such compounds[20, 21].

Computer chemistry methods have become a worthy tool to describe, classify materials and chemical reactions. One of the approaches used in a variety of corrosion studies is density functional theory (DFT)[22-25]. DFT is used to measure quantum chemical parameters, to classify characteristics of the corrosion mechanism inhibitor activities, and to analyze the interplay of inhibitor and the metal surface[26-30]. The theoretical estimate is very important since it is reliable and cost-effective. Theoretical calculations models give outcomes without time and potential, also they have a high economic value. Nevertheless, it is important to prove that these theoretical findings have been achieved by simple test results[31-33].

The aim of this study was the rapid synthesis of two molecules containing 1,2,4-triazole. Quantum chemical calculation was used for characterization molecule to improve the experimental section. In order to gain insight into the mechanism of corrosion inhibition and then to model the adsorption mode of the inhibitor on the metal surface, molecular orbital calculations were carried out to find good theoretical parameters to describe the inhibition property of inhibitors.

Experimental Details

The Infrared spectra were determined with a Perkin-Elmer Spectrum one FT-IR spectrophotometer, both ^{1}H- and ^{13}C-NMR spectra were recorded using the Bruker AC-400 NMR spectrometer operating at 400 MHz for ^{1}H-NMR, 100 MHz for ^{13}C-NMR. Compounds were dissolved in dimethyl sulfoxide and chemical shifts were referred to as TMS (Tetramethylsilane) for both ^{1}H- and ^{13}C-NMR. The Thomas Hoover melting point apparatus used for determining the melting points. The chemical compounds were procured from Aldrich Merck.

Procedure for synthesis compound I and II

The reaction was prepared using a two-mouthed 100 mL reaction flask, thermometer, reflux, and magnetic fish. 10 mmol of thiophene-2-carbohydrazide and 50 mL of absolute ethyl alcohol were added to the reaction flask. After the reflux process started, 10 mmol (phenyl isothiocyanate for the compound I) or (ethyl isothiocyanate for compound II) was added. After about 4 h, solid thiosemicarbazide started to form in the reaction flask. 15 mmol KOH was added to the solid and then dissolution was initiated. After 6 h, the reaction was stopped and pH was controlled between 3-4 precipitate formations. The formed solid was filtered, washed with ice water, and crystallized in an alcohol-water mixture. The structure of the obtained product was determined by FT-IR, ^{1}H-NMR, ^{13}C-NMR techniques. The general reaction of the product is given in (Scheme 1).

Characterization of 4-phenyl-5- (2-thiophene) -2,4-dihydro-3H-1,2,4-triazole-3-thiol (I)

Yield 70%; m.p.: 163-164°C; FT-IR (KBr, cm-1,): 3038-3104 (Ar-H), 1573 (C = N), 1259 (C = S), 681 (C-S-C), 1611, 1472, 1420(C-N, C=N, C-N-C in triazole) respectively; ^{1}H NMR (400 MHz, DMSO-d6, ppm): 6.65-7.71 (8H, Ar-H), 13.99 (s, 1H, SH); ^{13}C NMR (100 MHz, DMSO-d6, ppm): 117.33, 126.83, 128.70, 129.36, 130.21, 132.01, 146.65, 168.19. Molecular Weight: 259 (C12H9N3S2). Elemental analysis (theoretical): C, 55.57; H, 3.50; N, 16.20. S, 24.73; experimental, C, 55.56; H, 3.49; N, 16.19. S, 24.74.

Characterization of 4-Ethyl-5-(thiophene-2-yl)-4H-1,2,4-triazole-3-thiol (II)

Yield 84%;m. p.: 187-188°C; FT-IR (KBr, cm^{-1}, υ): 3072-3107(Thiophen group) 2870-2960 (C-H), 1570 (C=N), 1263 (C=S), 715 (C-S-C); ^{1}H NMR (400 MHz, DMSO-d_6, δ, ppm): 1.23 t (3H, N-CH_2-CH_3, J = 7.2

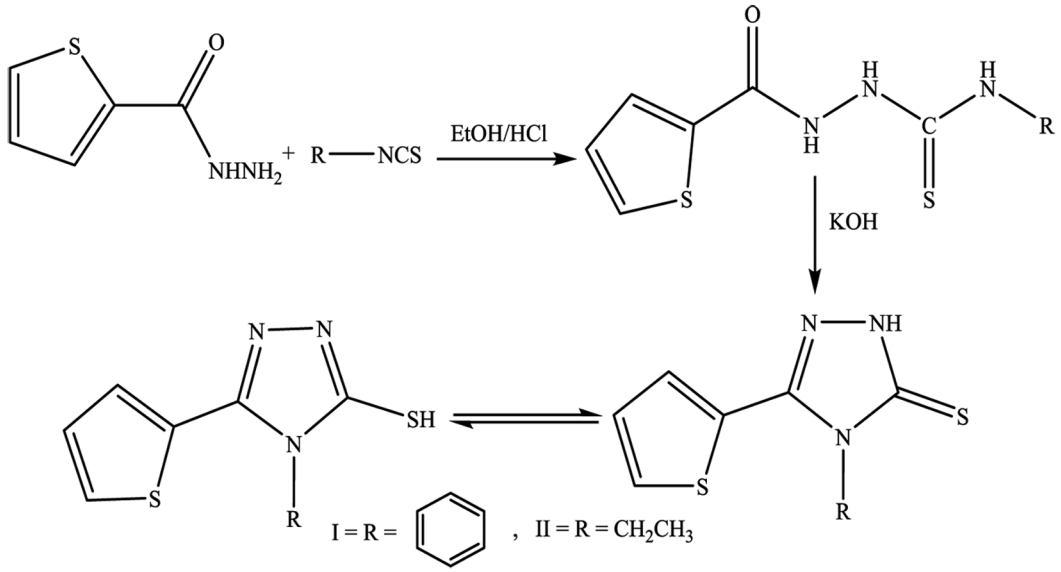

Scheme 1 — Synthesis of the title compounds

Hz), 4.22 q (2H, -N-CH_2-CH_3, J = 7.2 Hz), 7.27 dd (1H, Thio-H, J = 4.0, 4.8 Hz), 7.68 d (1H, Thio-H, J = 3.2 Hz) 7.86 d (1H, Thio-H, J = 4.8 Hz), 13.98 s (1H, SH); ^{13}C-NMR (100 MHz, DMSO-d_6, δ, ppm): 13.7, 39.7, 126.8, 128.9, 129.3, 130.3, 146.3, 167.5. Molecular Weight: 211 (C8H9N3S2). Elemental analysis (theoretical): C, 45.46; H, 4.28; N, 19.88. S, 30.34; experimental, C, 45.44; H, 4.25; N, 19.9. S, 30.32.

Computational Details

Computational calculations have been performed using the Gaussian program version 09[34, 35]. In the analytical gradients of Gaussian 09, the ground-state and excited-state geometries were optimized using the DFT method and the B3LYP correction with the cc-pVDZ basis collection set was utilized for the computation[36, 37]. The title compound was optimized and parameters, including bond length, bond angle, and dihedral angles were obtained using the same theory levels[38].

The electronic spectrum of the compounds was measured at DFT/B3LYP/cc-pVDZ in a gas phase. The stationary points are known as the minimum possible hypersurfaces of energy and have been verified by the absence of any imaginary frequency. For the basic vibrational modes with the corresponding IR intensities and the related overtones, the anharmonic frequencies were computed. Using NBO review, a full charge distribution was carried out[39, 40], and absorption spectra were taken with the same computational process.

The electronic structure markers have been determined from geometry-optimized structures and E_{HOMO}, E_{LUMO}, ΔE, σ, χ, nucleophilicity (ε) index, electrophilicity (ω) index, chemical potential (Pi), μ, and ΔN relevant to the action of corrosion inhibition were calculated. The negative charge distribution parameter is also investigated in addition to the electronic structure identifiers. Additionally, for the title compound, molecular electrostatic potential surface (MEP) and boundary molecular orbital (FMO) was investigated.

Result and Discussion

Structure optimization

For the optimized compounds the bond length, bond angle, and dihedral angle using the B3LYP/cc-pVDZ process were determined. (Fig. 1) reveals the atomic numbering configuration of the samples. For compound I, the theoretical bond length of N^4-C^1, C^6-C^1, C^{14}-N^3, and S^{25}-$C^2$are 1.319, 1.452, 1.433, and 1.769 Å, respectively; while for compound II, are 1.321, 1.453, 1.463, and 1.771 Å, respectively; on the other hand, the corresponding parameters obtained from the experimental results [33]are equal to 1.331, 1.348, 1.571, and 1.608 Å, respectively. For compound I, the bond angle between the atoms of C^6-C^1-N^4, S^8-C^6-C^1, and C^{14}-N^3-C^2 were theoretically found as123.6171º, 128.4706º, 126.173º; while for compound II, the corresponding parameters are 123.132, 117.345, 126.444; likewise, the practical result for the aforementioned bonds are equal to 123.6171, 130.91, and 125.44. Furthermore, the relation between theoretical (our title compound) and experimentally (related compound) result in a dihedral angle is listed in Table 1.

FT-IR spectra

FT-IR spectra for both title compounds are shown in (Fig. 2). The harmonic vibrational frequencies of the title compound were determined using B3LYP/cc-pVDZ. The vibrational band assignments were made by the molecular visualization software[41]. We evaluated the vibrational frequencies to promote the allocation of the observed peaks and to compare our title compounds with the corresponding experimental findings (Table 2). Generally, the experimental

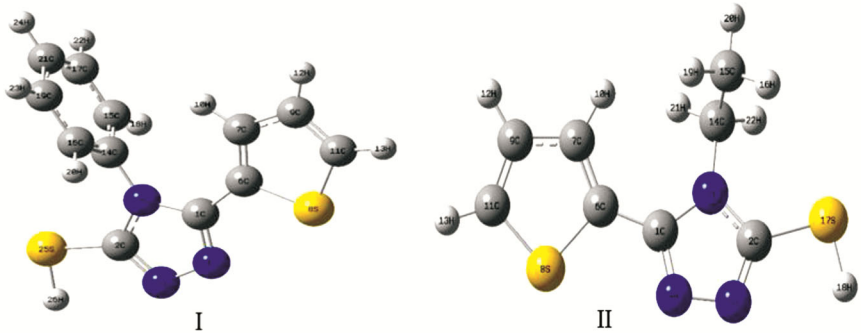

Fig. 1 — Geometrical structure for both title compounds optimized by B3LYP/cc-pVDZ

Table 1 — The geometrical optimization (Bond Length, Bond angle, and Dihedral angle) for both title compound with experimentally related compounds [33]

Compound I		Compound II		
Symbol	Bond Length (theoretical) (Degree)	Symbol	Bond Length (theoretical) (Degree)	Bond length (Experimental) (Degree)
C2-C1	2.1786772	C2-C1	2.1687395	
N3-C2	1.3790162	N3-C2	1.373741	
N4-C1	1.3195233	N4-C1	1.3217186	1.331
N5-C2	1.3133187	N5-C2	1.3150655	
C6-C1	1.4521444	C6-C1	1.4539483	1.348
C7-C6	1.3813619	C7-C6	1.3821809	
S8-C6	1.756448	S8-C6	1.7551094	
C9-C7	1.4259493	C9-C7	1.4261237	
C11-C9	1.3712216	C11-C9	1.3710587	
C14-N3	1.4338129	C14-N3	1.4631606	1.571
C15-C14	1.3994295	C15-C14	1.5289936	
C16-C14	1.3995394			
C17-C15	1.3970969			
C19-C16	1.3968625			
C21-C17	1.3985599			
S25-C2	1.7694527	S17-C2	1.7716265	1.6081
Symbol	Bond angle (theoretical)	Symbol	Bond Angle (theoretical)	Bond angle (experimental)
N3-C2-C1	38.38582	N3-C2-C1	38.490255	
N4-C1-N3	109.4502	N4-C1-C3	109.7605834	
N5-C2-C1	72.83871	N5-C2-C1	73.0485606	
C6-C1-N4	123.6171	C6-C1-C4	123.1328829	124.56
C7-C6-C1	131.6863	C7-C6-C1	132.0263023	
S8-C6-C1	128.4706	S8-C6-C1	117.345034	130.91
C9-C7-C6	113.0243	C9-C7-C6	113.2098902	
C11-C9-C7	112.7315	C11-C9-C7	112.6485749	
C14-N3-C2	126.173	C14-C3-C2	126.444081	125.44
C15-C14-N3	119.627	C15-C14-C3	113.324396	
C16-C14-N3	119.6614			
C17-C15-C14	119.4661			
C19-C16-C14	119.4519			
C21-C17-C15	120.1354			
S25-C2-C1	160.7683	S17-C2-C1	161.3180644	
Symbol	Dihedral angle (theoretical)	Symbol	Dihedral angle (theoretical)	Dihedral angle (experimental)
N4-C1-N3-C2	0.0042104	N4-C1-C3-C2	-0.3908311	
N5-C2-C1-N4	0.0276386	N5-C2-C1-C4	-0.0801968	
C6-C1-N4-N5	-179.9822662	C6-C1-C4-C5	178.4867438	−178.04
C7-C6-C1-N4	177.369649	C7-C6-C1-C4	160.2967787	
S8-C6-C1-N4	-2.2837793	S8-C6-C1-C4	-18.0367205	
C9-C7-C6-C1	-179.7048336	C9-C7-C6-C1	-178.675422	−176.72
C11-C9-C7-C6	0.0102346	C11-C9-C7-C6	0.1655893	
C14-N3-C2-C1	-179.3893232	C14-C3-C2-C1	-177.1219056	
C15-C14-N3-C2	-87.1028253	C15-C14-C3-C2	-88.2384596	
C16-C14-N3-C2	92.2953911			
C17-C15-C14-N3	179.784401			
C19-C16-C14-N3	-179.8741257			
C21-C17-C15-C14	-0.0393118			
S25-C2-C1-N4	179.903672	S17-C2-C1-C4	179.2913445	178.81

Table 2 — Comparison of the vibrational spectra between theoretical and experimental results

Atoms Compound I	Theoretical Vibration assigned I	Experimental Vibration assigned I	Atoms Compound II	Theoretical Vibration assigned I	Experimental Vibration assigned I
S,ST,V C11-H13, C9-H12, C7-H10	3250.02	3252	S,ST,V C11-H13, C9-H12, C7-H10	3250.10	
UN,ST,V C7-H10, C11-H13	3242.46	3243	UN,ST,V C7-H10, C11-H13	3235.18	
UN,ST,V C11-H13, C9-H12, C7-H10	3212.22		S,ST,V C11-H13, C9-H12, C7-H10	3211.85	
ST,V Ar-H	3212.11	3104 - 3038	S,ST C15-H19,H16;C14-H22,H21	3130.57	
ST,V Ar-H	3208.71		UN,ST C15-H20,H16,H19	3121.31	
ST, V Ar-H	3200.35		ST C14-H21,H22	3108.70	
ST,V S25-H16	2677.59	2677	S,ST C14-H21,H22	3061.59	
S, ST,V C=C in ring	1650.43	1651	S,ST C15-H16,H19,H20	3042.25	2870-2960
ST,V C1-N3 in Triazole	1611.49	1603	ST,V S17-H8	2682.65	
ST,V C14-N3	1529.96	1573	UN,ST,V C7=C6,C9=C11	1610.45	
ST,V C11=C9	1520.87	1521	ST,V C11=C9	1522.01	
ST,V C=C in ring	1478.76	1479	Si,ST,V C14-H21,H22	1496.03	
ST,V C2=N5	1472.91		Si,ST,V C15-H16,H19	1479.86	
ST,V C7-C9	1467.64		ST,V C2=N5	1470.67	
S, ST, C2=N5-C	1420.28	1417	RO,V C15-H16,H19,H20	1463.07	
ST,V C=N in Triazole	1472.87	1468	ST,V C=N in Triazole	1461.06	1570
UN,ST,V C11-H13, C7-H18, C9-H12	1366.17		ST,V C=N in Triazole	1424.50	
UN,ST,V C=C in ring	1355.08		UN,ST,V C15-H16,H19	1403.76	
UN, ST,V Triazole ring	1346.47		UN, ST,V Triazole ring	1397.37	
RO,V H in ring	1322.88		Si,ST,V C14-H21,H22	1379.73	
ST,V C2-S25	1298.57	1259	ST,V C14-H21,H22	1299.10	
S, ST,V Ar-H	1183.69		ST H in Thiophene	1235.92	1260
ST,V N-N-H	1120.43		ST,V H in ethane group	1153.65	
S, ST,V Ar-H	1095.2		ST,V N4-N5	1110.75	
Si, ST,V C11-H13, C9-H12	1091.38		RO C15-H16,H19	1099.33	
Si,ST,V C11-H13, C7-H18	1078.93	1078	Si,ST,V C11-H13,C9-H12	1089	
Si,ST,V C9-H12, C7-H18	1061.4		Si,ST,V C11-H13, C7-H18	1075.17	
TW,V Ar ring	1020.73	1017	ST,V ethane group	977.35	
UN,ST,V C=C in ring	1015.7		V of All atoms	950.91	
UN, ST,V Ar-H	992.38		ST,V S17-H18	905.82	
RO,V S25-H26	911.57		ST,V S8-C11	851.81	715
UN, ST,V N3-C1-N4	719.58		UN,ST,V N3-C1N4	721.77	
RO, ST,V C11-H13	709.62		RO,ST, C11-H13	710.6	
ST,V Thiophene	656.6	681	ST,V Thiophene	645.49	
RO,V S25-H26	243		ST,V S17-H18	234.74	

S; stretching, V; Vibration, ST; symmetrical, UN; Unsymmetrical, Si; Sisering; RO; Rocking

frequencies are satisfied by the theoretical calculations. The bands determined in the range of 4000-400 cm^{-1} measured area emerge from the vibrations of both title compounds, including the vibration of N-H, C-N, C-S and C=C, Ar-H stretching, and the internal vibrations, etc. The stretching modes of C-N, C=N, and C-N-C for the Triazole, theoretically were observed as 1611.49, 1472.91, and 1420.28 cm^{-1}, whereas experimentally the corresponding parameters have been reported as1603, 1468, and 1417, respectively.

In Compound I, the three hydrogens in the thiophene group have strong stretching modes, which theoretical were obtained as 3250 and 3242 cm^{-1} while having experimentally recorded as 3252 and 2243cm^{-1}. On the other hand, for compound II, the important peak can be seen for C-H, C=N, C=S, and C-S-C at 2870-296, 1570, 1260, and 715ppmin the reported experimental results, but from the theoretical calculation, the corresponding peaks are 3042.25, 1461.06, 1235.92 and 851.81, respectively. Also, Table 3 listed other computational parameters for both compounds. The two facts could be attributable to the difference between the observed and measured frequencies; firstly, for the practical one, the compound has a solid-phase, while in the theoretical computation they assumed as gaseous phase; the second reason can be contrary to the experimental values reported in the presence of intermolecular interactions, while the calculations were performed on a single molecule. The transition strength was determined using the infrared intensity (rel. intensity)

Table 3 — Theoretical and experimental ^{1}H and ^{13}C chemical shift concerning TMS, where all values in ppm, for title compound.

Atom	Compound I Experimental (ppm) (DMSO-d6)	Calculated (ppm) B3LYP/cc-pVDZ	Atom	Compound II Experimental (ppm) (DMSO-d6)	Calculated (ppm) B3LYP/cc-pVDZ
C7,C9	117.33	130.45, 133.1	C15	13.7	25
C15,C16	126.83	135.8	C14	39.7	50.2
C17,C19	128.7	137.5	C7	126.8	130.1
C21,C11	129.36	138.5,139.7	C9	128.9	133.7
C14	130.21	142.5	C11	130.3	140.2
C6	132.01	144.8	C6	146.3	145.6
C1	146.65	158.5	C1	168.5	159.33
C2	168.19	161.2	C2		160.43
8H, Ar-H	6.65-7.71	7.15-8.98	3H for CH3	1.23	2.6-2.8
1H, SH	13.99	5.5	2H for CH2	4.22	4.9-5.3
			S-H	13.98	5.6
			H for Thiophene group	7.27-7.86	8.4-8.5

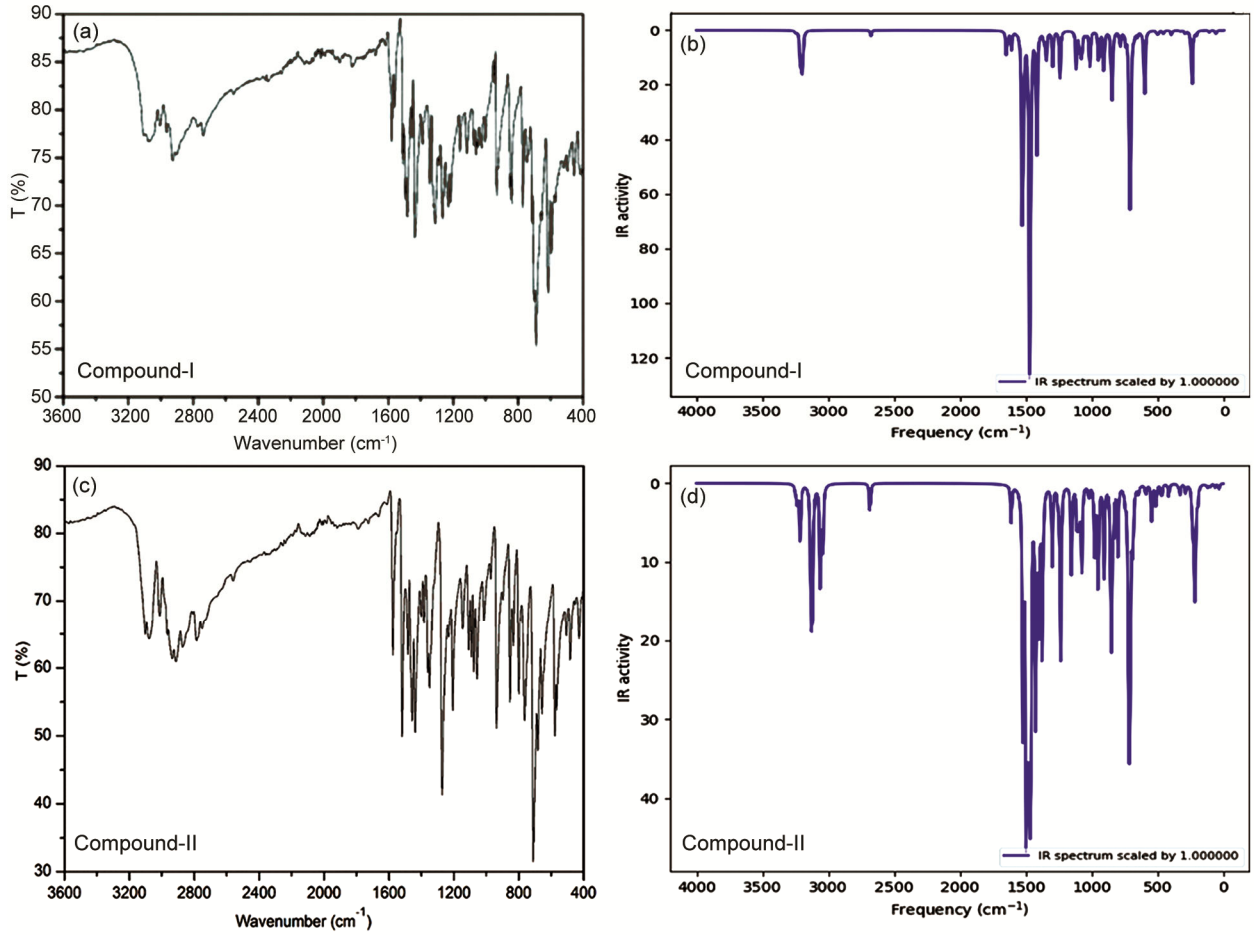

Fig. 2 — IR spectra of the title compound for the (a,c) experimental and (b,d) theoretical result

results. It is noticed that the intensity of IR spectra is usually recorded as transmission or absorbance percentage, which is displayed in (Fig. 2).

Nuclear magnetic resonance spectra

The measurement of GIAO ^{1}H and ^{13}C chemical shift values (concerning TMS), the B3LYP approach with a cc-pVDZ basis set was used, which was then contrasted with the experimental ^{1}H and ^{13}C chemical shift values. The results of the analysis are listed in Table 4. At B3LYP/cc-pVDZ stage, we have measured ^{1}H chemical shift values (concerning TMS) of 9.00-0.00 ppm, while its couponing value has been reported as 14.80-0.8 ppm. For the compound I, the

Table 4 — Quantum chemical calculated parameters for the studied compounds

Molecule Name	Equations	Compound I	Compound II
Total Energy (a.u)		-1423.3721	-1270.9372
μ (D)		5.5150	4.8520
ELUMO (eV)		-1.2054	-1.2215
EHOMO (eV)		-5.7122	-5.8091
ΔE (eV)	$\Delta E = (EHOMO - ELUMO)$	4.5067	4.5876
I	$I = -E_{HOMO}$	5.7122	5.8091
A	$A = -E_{LUMO}$	1.2054	1.2215
χ (eV)	$\chi = (I + A) / 2$	3.4588	3.5153
η (eV)	$\eta = (I - A) / 2$	2.2533	2.2938
σ (eV)	$\sigma = 1/\eta$	0.4437	0.4359
Pi (eV)	$Pi = -\chi$	-3.4588	-3.5153
ω (eV)	$\omega = Pi^2/2\eta$	2.6546	2.6936
ε (eV	$\varepsilon = Pi.\ \eta$	-7.7941	-8.0634
ΔN	$\Delta N = (\chi_{metal} - \chi_{inhibitor}) /2. (\eta_{metal} - \eta_{inhibitor})$	0.7857	0.7595

aromatic protons experimentally observed at 6.65-7.71 ppm, while the computational value is found as 7.15-8.98 ppm. For the compound II, the H for methyl group theoretically was observed at 2.6-2.8 ppm while the reported experimental result is 1.23 ppm.

For compound I, the experimentally S-H has appeared at 13.99 ppm while computed appeared at 5.5 ppm, but for compound II, it is at 5.6 ppm.This difference between experimental and theoretical chemical shifts for S-H has been observed because the intermolecular hydrogen bonds in title molecular structure are ignored in the theoretical calculation. The measured ^{13}C chemical shift values (with regard to TMS) of B3LYP/cc-pVDZ are between 0.00-180.00 ppm, while the experimental results were scaled in the range of 0.00-200 ppm. Theoretical ^{1}H and ^{13}C chemical change outcomes of the title compound are usually closer to the experimental chemical, as can be seen in Table 3.

Inhibitor activity parameters

The electronic structure identification, derived from the molecular electro-structure, which is associated with the electronic structure, includes E_{HOMO}, E_{LUMO} which were obtained from the output file of the Gaussian program. Additionally, energy bandgap (ΔE_{gap}), softness (σ), hardness (η), electronegativity (χ), electrophilicity (ω), chemical potential (Pi), nucleophilicity (ε), HOMO, LUMO, and dipole moment (μ). were calculated according to the following equations[42-45]:

$$I = -E_{HOMO} \quad \ldots(1)$$
$$A = -E_{LUMO} \quad \ldots(2)$$
$$\Delta E = (E_{LUMO} - E_{HOMO}) \quad \ldots(3)$$
$$\eta = (I - A) / 2 \quad \ldots(4)$$
$$\sigma = 1/\eta \quad \ldots(5)$$
$$\chi = (I + A) / 2 \quad \ldots(6)$$
$$Pi = -\chi \quad \ldots(7)$$
$$\omega = Pi^2/2\eta \quad \ldots(8)$$
$$\varepsilon = Pi.\ \eta \quad \ldots(9)$$

The electronic transfer between inhibitor and metal can be identified by corrosion studies, which can be calculated from χ and η according to this equation[46]:

$$\Delta N = \frac{(\chi metal - \chi inhibitor)}{2.(\eta metal - \eta inhibitor)} \quad \ldots(10)$$

where $\chi_{inhibitor}$ and $\eta_{inhibitor}$ theoretically were calculated, while the χ_{metal} and η_{metal}were determined experimentally from the literature[47]. Pearson [47] stated that the electron affinity (A) and ionization potential (I) was equal to each other for a single metal (A=I), thus the η_{metal} is taken zero for the single metal. All-electronic structure parameters for the title compound are given in Table 4.

The inhibitory characteristic of the compounds was calculated by optimizing their bond lengths, bond angles, and dihedral angles, the geometric, and electronic structures of. Table 1 showed that the bond length between S-H for compound II (1.771 Å) is longer than compound I (1.769 Å). The S-H group has the best position for bonding the compounds on the metal surface. Both compounds showing weak bonds between S-H with a single bond character, and thus, they facilitate the adsorption of the inhibitor on the metal surface. Also, for compound II, N4-C1 with N5-C2 are another position, which the molecular inhibitor can react with metal surface. The bond length of N4-C1 and N5-C2 are a little be higher in the compound I, therefore itsinhibitor corrosion is less than the compound II.

The Mulliken charges results indicate negative charges on the atoms N and S in both compounds (I and II), which can be considered as the active centers

for the metal surface adsorption of the inhibitor. The charge distribution on the nitrogen atom for both compounds is very close to each other, also the charge on the S-H for compound II is higher than compound, which indicates that compound II has more anti-corrosion activity (Table 5).Therefore, due to the negatively charged nitrogen atoms and carbon in the Triazole ring, the compound II has an effective inhibition. From MEP map given in (Fig. 3), it can be seen that the nitrogen atoms (N3 and N4) in the Triazole ring in the compound II has denser red color, which represents the more negative charge compared with the compound I. Detail for the charge distribution for both molecules are nearly the same, it is the inhibitor for corrosion not more different.

E_{HOMO} is a quantum chemical description that often refers to the electron donation capacity of a molecule. The higher value of E_{HOMO} possibly indicates the tendency of the molecule to donate electrons to the required low empty molecular orbital energy (acceptor molecule). The energy of the lowest unoccupied molecular orbital (E_{LUMO}) shows the ability of a molecule to accept electrons. The lower the value of E_{LUMO}, the more likely it is to accept electrons from the molecule [48]. The inhibitor's binding capacity to the metal surface increases with increasing energy of HOMO and and/or decreasing the energy value of LUMO. Table 4 and (Fig. 4) show that the compound II, with -5.8091 eV, has the maximum HOMO energy, which means that it likes to be adsorbed by the lone pair of electrons of the sulfur atoms on the iron surface. This improves its adsorption on the metal surface, and thus, improves its inhibition effectiveness.(Fig. 4) displays the delocalization of the charge of the entire atoms in compound I reveals that the lowest LUMO energy amount is -1.2054 eV. This is why the inhibitor activity of compound I is close to that of compound II. It can be stated that compound II has a good inhibitor activity due to higher E_{HOMO}, also compound I has a similar inhibitor activity due to lower E_{LUMO}.

The separation energy, $\Delta E = (E_{LUMO} - E_{HOMO})$ is an important parameter because it shows the reactivity of an inhibitory of a molecule against adsorption on the metal surface. As ΔE decreases, the molecule's reactivity increases, and hence it can increase the efficiency molecular inhibition. Table 4, and (Fig. 4) show that, for compound I, the lowest calculated ΔE is 4.5067eV. This can cause it to be adsorbed on the metal surface and thus increase its inhibitory effect. Consequently, compound I has the highest dipole moment 5.5150 D, Table 1, which increases the probability of its adsorption on the metal surface and increases the efficiency of inhibition. Adsorption occurred can occur on the highest softness and lower hardness position of a molecule[49]. The calculations show that the maximum softness of the compound I to

Table 5 — Millikan atomic Charge distribution on the atoms

Compound I		Compound II	
Atoms	Charge	Atoms	Charge
C1	0.245209	C1	0.240591
C2	0.054684	C2	0.06143
N3	-0.22039	N3	-0.22633
N4	-0.19294	N4	-0.19336
N5	-0.17176	N5	-0.17524
C5	-0.14216	C6	-0.13675
C7	0.009542	C7	0.004398
S8	0.189179	S8	0.195831
C9	0.083671	C9	0.082356
C11	-0.11611	C11	-0.11517
C14	-0.01842	C14	0.048796
C15	0.083232	C15	-0.02186
C16	0.083012	S17	-0.03237
C17	0.050375		
C19	0.050256		
C21	0.041211		
S25	-0.01618		

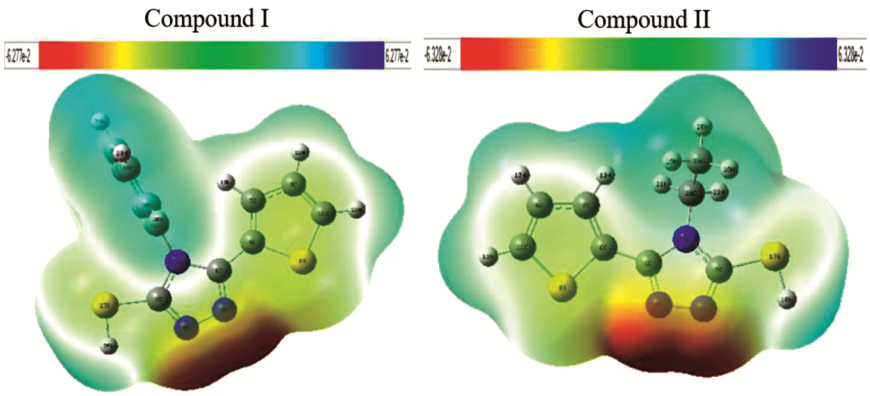

Fig. 3 — Molecular electrostatic potential map

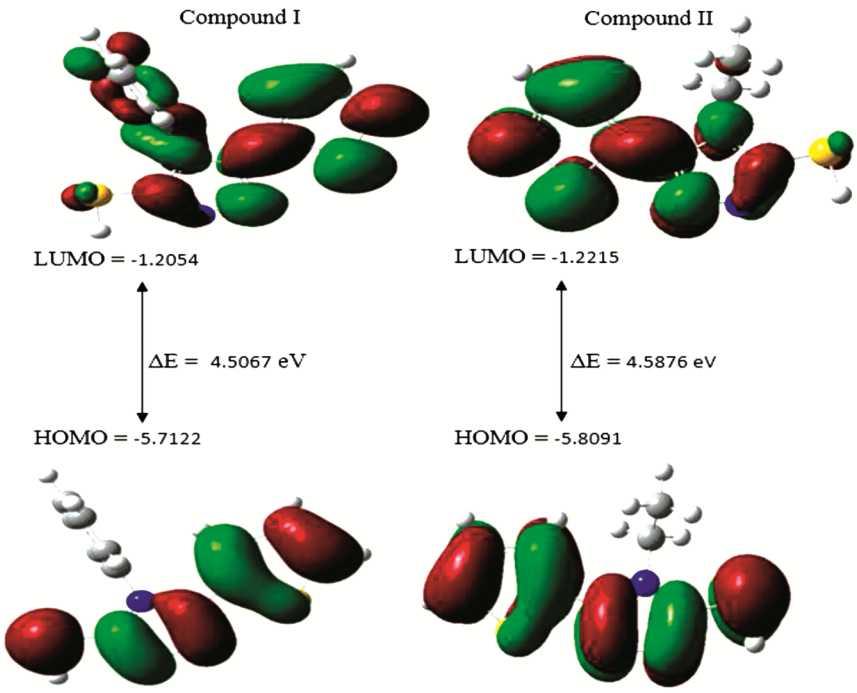

Fig. 4 — HOMO and LUMO energy level for both compounds

be 0.4437 with a lower hardness of 2.2533 compared with compound II.

Other parameters to be measured for inhibitor activity are χ and Pi. Calculated χ values provide details about how the coordinated covalent bond happens between the metal and the inhibitor[50]. This report investigated the corrosion inhibition behavior of the molecules intended as iron metal. It is found that the χ values of the inhibitors (Table 4) are smaller than their corresponding experimental values for the iron metal. The iron metal can form bonds with taking electrons from the inhibitor compound. The compound I serves as the most powerful corrosion inhibitor with the lowest χ value compared to the other compound. Pi is opposite to electronegativity, whereby a molecule with high chemical potential possesses a high activity. The ω and ε indices are major parameters used in corrosion inhibitor activities. The value of ω shows the capability of inhibitor molecules to accept electrons[51]. The ε index indicates the inhibitors' capacity to donate electrons[52]. The activity of inhibition increases as the ω value decreases or the ε value increases[53]. The calculated ω value for compound I decreased and the ε value increased, respectively. The inhibitor I have the most powerful inhibitory effect since the values of ω and ε in conjunction with other parameters. The measured electron transfer fraction, ΔN, indicates that most electrons transferred to the iron surface derive from the compound I molecule equal to 0.7857e.

Conclusion

In this study, the inhibition and some other properties of 4-phenyl-5-(thiophen-2-yl)-4H-1,2,4-triazole-3-thiol and 4-ethyl-5-(thiophen-2-yl)-4H-1,2,4-triazole-3-thiol were successfully investigated. The compounds were characterized with IR, ^{1}H NMR, and ^{13}C NMR spectral. A good correlation between experimental and theoretical data was observed. According to the obtained results, compound I has a higher value of E_{LUMO} and lower E_{HOMO} compared with the compound II. For this reason, it was determined that compound I is a good donor and had high inhibitor activity. It can be said that compound I has a stronger inhibition activity due to the lower ΔE. Since it has a higher dipole moment value, it can enhance the corrosion resistance of metals. From the atomic charges of the compound I, it was found that the electronegative atoms have a major influence on the action of inhibition. The most active area in the MEP map was around the Nitrogen(s) and sulfur (s) atoms in both compounds. The determined parameters, including η, ω, σ, ε, Pi and χ showed that the compound I has a powerful inhibitor affect against corrosion. An inhibitor with lower χ value means that the iron metal can form a bond by taking electrons

from the compound inhibitor. The higher value ΔN of the inhibitor indicates that the metal surface can be better adsorbed, therefore corrosion inhibition can be increased. As the number of heteroatoms in the structures increases, this compound will have a strong corrosion inhibition. Finally, both compounds are good candidate to be used as inhibitors for anti-corrosion.

Acknowledgement

This work was supported by Firat University Organic Lab working.

References

1 Schiff H, *Justus Liebigs Annalen der Chemie*, 131 (1864) 118.
2 Silva C M D, Silva D L D, Modolo L V, Alves R B, Resende M A D, Martins C V B & Fatima A D, *J Adv Res*, 2 (2011) 1.
3 Brodowska K & Łodyga-Chruścińska E, *Chemik*, 68 (2014) 129.
4 Prakash A & Adhikari D, *Int J ChemTech Res*, 3 (2011) 1891.
5 Zoubi W A, *Int J Org Chem*, 3 (2013) 73.
6 Gupta, K C & Sutar A K, *Cord Chem Rev*, 252 (2008) 1420.
7 Qin W, Long S, Panunzio M & Biondi S, *Molecules*, 18 (2013) 12264.
8 Ahmed M H O, Al-Amiery A A, Al-Majedy Y K, Kadhum A A H, Mohamad A B & Gaaz T S, *Results in Physics*, 8 (2018) 728.
9 Salman T A, Al-Amiery A A, Shaker L M, Kadhum A A H & Takriff M S, *Int J Corrosion and Scale Inh*, 8 (2019) 1035.
10 Al-Amiery A A, Shaker L M, Kadhum A A H & Takriff M S, *Tribology in industry*, 42 (2020) 89.
11 Al-Taweel S S, Al-Janabi K W S, Luaibi H M, Al-Amiery A A & Gaaz T S, *Int J Corrosion and Scale Inh*, 8 (2019) 1149.
12 Salman, T.A, Zinad D S, Jaber S H, Al-Ghezi M, Mahal A, Takriff M S & Al-Amiery A A, *Journal of Bio-and Tribo-Corrosion*, 5 (2019) 1.
13 Habeeb H J, Luaibi H M, Dakhil R M, Kadhum A A H, Al-Amiery A A & Gaaz T S, *Results in Physics*, 8 (2018) 1260.
14 Kadhim A, Al-Okbi A K, Jamil D M, Qussay A, Al-Amiery A A, Gaaz T S, Kadhum A A H, Mohamed A B & Nassir M H, *Results in Physics*, 7 (2017) 4013.
15 Al-Azawi K F, Mohammed I M, Al-Baghdadi S B, Salman T A, Issa H A, Al-Amiery A A, Gaaz T S & Kadhum A A H, *Results in Physics*, 9 (2018) 278.
16 Al-Baghdadi S B, Hashim F G, Salam A Q, Abed T K, Gaaz T S, Al-Amiery A A, Kadhum A A H, Reda K S & Ahmed W K, *Results in Physics*, 8 (2018) 1178.
17 Alobaidy A H, Kadhum A, Al- Baghdadi S B, Al-Amiery A A, Kadhum A H, Yousif E & Mohamad A B, *Int. J. Electrochem. Sci*, 10 (2015) 3961.
18 Zinad D S, Hanoon M, Salim R D, Ibrahim S I, Al-Amiery A A, Takriff M S & Kadhum A A H, *Int J Corros Scale Inhib*, 9 (2020) 228.
19 Jamil D M, Al-Okbi A K, Al- Baghdadi S B, Al-Amiery A A, Kadhim A, Gaaz T S, Kadhum A A H & Mohamad A B, *Chemistry Central Journal*, 12 (2018) 1-9.
20 Cang H, Fei Z, Shao J, Shi W & Xu Q, *Int J Electrochem Sci*, 8 (2013) 720.
21 Cohen S L, Brusic V A, Kaufman F B, Frankel G S, Motakef S & Rush B, *J Vac Sci & Tech A*, 8 (1990) 2417.
22 Mohamed M E B & Taha K K, *Am J Res Commun*, 3 (2015) 143.
23 Bhawsar J, Jain P K, Jain P & Bhawsar M R, *Asian J Res Chem*, 7 (2014) 386.
24 Peme T, Olasunkanmi L O, Bahadur I, Adekunle A S, Kabanda M M & Ebenso E E,.*Molecules*, 20 (2015) 16004.
25 Koparir P, Karaarslan M, Orek C & Koparir M, *Phosphorus, Sulfur & Silicon and the Related Elements J*, 186 (2011) 2368.
26 Mujica-Martínez C A & Arce J C, *Int J Quantum Chem*, 110 (2010) 2532.
27 Mehmeti V V & Berisha A R, *Frontiers in Chemistry*, 5 (2017) 61.
28 Anusuya N, Sounthari P, Jagadeesan S, Parameswari K & Chitra S, *Oriental J Chem*, 31 (2015) 1741.
29 Al-Amiery A, Salman T A, Alazawi K F, Shaker L M, Kadhum A A H & Takriff M S, *Int J Low-Carbon Tech*, 15 (2020) 202.
30 Chaouiki A, Lgaz H, Slaghi R, Gaonkar S L, Bhat K S, Jodeh S, Toumiat K & Oudda H, *Portugaliae Electrochimica Acta*, 37 (2019) 1.
31 Hussein R K, Abou-Krisha M & Yousef T A, *Biointerface Res Applied Chem*, 11 (2020) 9772.
32 Koparir P, Sarac A, Orek C & Koparir M, *J Mol Struct*, 1123 (2016) 407.
33 Cansız A, Orek C, Koparir M, Koparir P & Cetin A, *Spectrochim Acta A Mol Biomol Spectrosc*, 91 (2012) 136.
34 J. E. Carpenter and F. Weinhold, *J Mol Struct (Theochem)*, 139 (1988) 41.
35 Ahmed L & Omer R, *Cumhuriyet Science Journal*, 41 (2020) 916.
36 Chibani S, Jacquemin D & Laurent A D, *Comput Theor Chem*, 1040 (2014) 321.
37 Omar R A, Koparir P, Ahmed L O & Koparir M, *Turkish Computational and Theoretical Chemistry*, 4 (2020) 67.
38 Shahab S, Almodarresiyeh H A, Kumar R & Darroudi M, *J Mol Struct*, 1088 (2015) 105.
39 Elshakre M & Sadiek I, *Comput Theor Chem*, 1088 (2016) 32.
40 Ahmed L & Omer R, *J Phys Chem Functional Mat*, 3 (2020) 48.
41 Charef Tabti & Nadia Benhalima, *Advances in Materials Physics and Chemistry*, 5 (2015) 221.
42 Koopmans T, *Physica*, 1 (1933) 104.
43 Plakhutin B N & Davidson E R, *J Phys Chem A*, 113 (2009) 12386.
44 Jesudason E P, Sridhar S K, Malar E J P, Shanmugapandiyan P, Inayathullah M, Arul V, Selvaraj D & Jayakumar R, *Eur J Medi Chem*, 44 (2009) 2307.
45 Gökce H & Bahceli S, *Spectrochim Acta A Mol Biomol Spectrosc*, 79 (2011) 1783.
46 Musa A Y, Jalgham R T & Mohamad A T, *Corrosion Science*, 56 (2012) 176.
47 Pearson R G, *Inorganic Chemistry*, 27 (1988) 734.
48 Özcan M, Dehri I & Erbil M, *Applied Surface Science*, 236 (2004) 155.
49 Issa R M, Awad M K & Atlam F M, *Applied Surface Science*, 255 (2008) 2433.
50 Beytur M, Irak Z T, Manap S & Yuksek H, *Heliyon*, 5 (2019) e01809.
51 Kiyooka S-I, Kaneno D & Fujiyama R, *Tetrahedron*, 69 (2013) 4247.
52 Kariper S E, Sayın K & Karakaş D, *Hacet J Biol Chem*, 42 (2014) 337.
53 Karakus N & Sayin K, *J Taiwan Inst Chem Eng*, 48 (2015) 95.